The novel anti-neuroblastoma agent PF403, inhibits proliferation and invasion *in vitro* and in brain xenografts

CHAO LI[1], YAN LI[1], HAINING LV[1], SHAOWU LI[2], KE TANG[1], WANQI ZHOU[1], SHISHAN YU[1*] and XIAOGUANG CHEN[1*]

[1]Institute of Materia Medica, Chinese Academy of Medical Sciences and Peking Union Medical College, Beijing; [2]Department of Neurosurgery, Capital Medical University Affiliated Beijing Tiantan Hospital; Beijing Neurosurgical Institute, Beijing 100050, P.R. China

Received October 22, 2014; Accepted December 20, 2014

DOI: 10.3892/ijo.2015.2977

Abstract. Neuroblastoma is the most common cancer in infants and the fourth most common cancer in children. Our previous study showed that PF403 had a potent antitumor ability. In the present study, we evaluated the anti-neuroblastoma property of PF403 and investigated the underlying mechanisms. MTT assay, colony formation assay and flow cytometry assay were used to assess cytotoxicity of PF403 on SH-SY5Y cells. Transwell assay was chosen to estimate the anti-invasion ability of PF403 on neuroblastoma cells. The protein expression was detected by western blot analysis. The SH-SY5Y brain xenograft model was used to assess *in vivo* antitumor activity of PF403. PF403-mediated SH-SY5Y cell death was found to be dose- and time-dependent, and PF403 was able to limit invasion and metastasis of neuroblastoma cells. MRI and pathology analysis proved that the pro-drug of PF403, CAT_3, inhibited SH-SY5Y cells *in vivo*. PF403 decreased expression of phosphorylated FAK, MMP-2 and MMP-9 proteins, and downregulated the activity of PI3K/AKT and Raf/ERK pathways, followed by regulation of the proteins expression of Bcl-2 family, activated caspase-3, -9 and PARP and initiation of apoptosis of neuroblastoma cells. PF403 exerted cytotoxicity against SH-SY5Y neuroblastoma cell both *in vitro* and *in vivo*, and inhibited its invasion ability, suggesting PF403 has potential as a new anticancer drug for the treatment of neuroblastoma.

Correspondence to: Professor Xiaoguang Chen or Professor Shishan Yu, Institute of Materia Medica, Chinese Academy of Medical Sciences and Peking Union Medical College, 2 Nanwei Street, Xicheng, Beijing 100050, P.R. China
E-mail: chxg@imm.ac.cn
E-mail: yushishan@imm.ac.cn

*Contributed equally

Key words: neuroblastoma, orthotopic implantation, MRI, apoptosis, invasion

Introduction

Neuroblastoma (NB) is a common childhood malignant tumor of neural crest origin, generated in the paravertebral sympathetic ganglia and the adrenal medulla. NB is also the most common extracranial solid tumor in children (>7% of tumors in patients younger than 15 years) and a major cause of neoplastic death in infancy (15% of deaths in pediatric oncology) (1). Current surgery and radiotherapy in conjunction with chemotherapy has greatly improved survival rates for the patients with low-risk and intermediate-risk NB. However, high-risk patients still have an overall survival rate of <40% despite intensive therapy (2). Thus, it is urgent to develop new drugs for the treatment of high-risk NB.

Phenanthroindolizidine and phenanthroquinolizine alkaloids are family of plant-derived alkaloids composed of more than sixty compounds (3). The biological properties of these alkaloids include cancer cell growth inhibition (*in vitro* and *in vivo*), anti-inflammatory activity, anti-ameobicidal and anti-viral activity (4-6). Our previous studies show that (+)-13a-(S)-Deoxytylophorinidine (CAT) (Fig. 1A) had potent antitumor activity both *in vivo* and *in vitro* (7,8). Furthermore, 3-O-Desmethyl-13a-(S)-deoxytylophorinine (PF403) (Fig. 1B), one of CAT *in vivo* metabolites, showed stronger proliferation inhibitory activity than CAT on several tumor cell lines (9).

In the present study, we investigated the anti-neuroblastoma potential of PF403 in human NB cell line and in an *in vivo* NB mouse model. Since our previous studies on pharmacokinetic had proved poor bioavailability of PF403, the pro-drug of PF403, CAT_3, was chosen to study anti-neuroblastoma activity *in vivo* (8). Both MRI and pathology analysis verified the anti-neuroblastoma ability of PF403 *in situ*. Then mechanisms of PF403 on anti-neuroblastoma were studied. Collectively, our results for the first time addressed multiple mechanisms associated with PF403-mediated neuroblastoma cell death and suggested the possible application of PF403 for neuroblastoma therapy.

Materials and methods

Cells and chemicals. SH-SY5Y cell line was obtained from the cell center of CAMS&PUMC. The cells were maintained

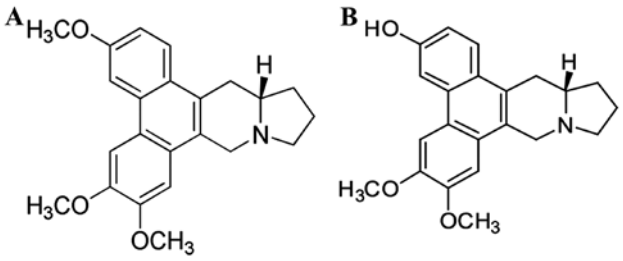

Figure 1. Chemical structure of (A) CAT and (B) PF403.

in Dulbecco's modified Eagle's medium (DMEM; Invitrogen, Carlsbad, CA, USA) supplemented with 10% fetal bovine serum (FBS; Gibco, Waltham, MA, USA), 100 IU/ml penicillin and 100 μg/ml streptomycin (Invitrogen) in a humidified incubator containing 5% CO_2 at 37˚C. PF403 and CAT_3 were obtained from the research group of Professor Shi-shan Yu (Institute of Materia Medica, China).

Cell viability assay. SH-SY5Y cells were seeded in a 96-well plate. After 24 h, the cells were treated with different concentrations of PF403. After 48, 72 and 96 h of incubation, cells were incubated with 1 mg/ml of MTT (Sigma, St. Louis, MO, USA) for 4 h at 37˚C in a CO_2 incubator. Mitochondrial reduction of MTT to formazan was determined. Amount of formazan was measured by absorbance at 570 nm with reference wavelength at 450 nm. IC_{50} values were calculated and expressed as mean ± standard deviation of three independent experiments.

Colony formation assay. The cells were seeded at a density of 200 cells/ml into 6-well culture plates for 24 h, then washed with phosphate-buffered saline (PBS) and cultured by DMEM with a series concentration of PF403 added. Colonies were allowed to grow for 14 days. After removing the medium, each well was carefully washed twice with PBS. The cells were fixed in methanol for 15 min and then stained with crystal violet for 20 min. Finally, positive colony formation (>50 cells per colony) was counted.

Flow cytometry assay. Cells were treated with a different of concentrations of PF403. After 72 h of treatment, cells were fixed with 70% ethanol, stained with propidium iodide (PI), and were analyzed by flow cytometry. The data were analyzed with CellQuest Pro software (BD Biosciences, San Jose, CA, USA). The experiments were repeated at least three times.

Invasion assay. Matrigel (10 μl) (BD Biosciences), a reconstituted basement membrane, was pre-coated on the upper compartment of Millicell (Millipore, Billerica, MA, USA) containing 8-μm pores. Approximately 600 μl of DMDM with 10% FBS was added to the lower compartment; 200 μl of the completed medium containing $2x10^5$ SH-SY5Y cells were seeded to the upper compartment. PF403 was added to the upper compartment at a series of concentrations. After culturing for 24 h at 37˚C in a humidified 5% CO_2, cells migrated to the lower compartment were stained and counted under the microscope.

Pharmacokinetic analyses. Animals (Vital River Laboratories, Beijing, China) were randomly assigned to ten groups (n=3/group) that were given a single dose of CAT_3 (10 mg/kg) orally. Mice were decapitated following 5, 15, 30 min, 1, 2, 4, 6, 8, 12 and 24 h. Brain structures were dissected on dry ice. Brain tissue homogenate with PF403 (5, 10, 25, 100, 250, 500, 1,000 and 2,500 ng/ml) of blank group was used as standard solution. High performance liquid chromatography (HPLC) system Agilent 1100 Series (Agilent Technologies, Santa Clara, CA, USA), equipped with a binary pump, an autosampler and degasser. Separation was performed using a Zorbax C18 column (2.1x100 mm, 3.5 μm). The column was thermostated at 25˚C. The optimized mobile phase solvents were: 0.1% formic acid/water =35/65. CAT_3 and its metabolites were separated at a flow rate of 0.2 ml/min with a linear gradient. Mass spectral data were obtained in positive electrospray mode. High purity nitrogen used as a sheath gas, was generated with a nitrogen generator. The m/z of PF403 was 350.1-281. Levels of CAT_3 and its metabolites were calculated using the calibration standard curves, constructed by linear regression analysis of peak area vs. concentration curves. CAT_3 and PF403 (2 μl) incubated with hepatic microsome, plasma, artificial intestinal or artificial gastric juice at 37˚C for 15 or 20 min. LC/MS analyzed concentration of CAT_3 and PF403.

Animals and surgical technique. Five-week-old female Balb/c nude (nu/nu) mice (Vital River Laboratories) were housed in standard facilities and given free access to water and rodent food. All animal experiments in the present study were conducted according to the guidelines of the Law for The Care and Welfare of Animals in China and approved by the Animal Experiment Committee of Institute of Materia Medica. For intracranial injection, mice were anesthetized with pentobarbital sodium (i.p) in a dosage of 50 mg/kg, placed in a stereotaxic restrain, and a small surgical incision was made in the skin covering the skull 2 mm to the right of the bregma. Cell suspensions (5 μl) containing ~$5x10^5$ SH-SY5Y cells were slowly (~30 sec) injected intracranially at 2.5 mm below the skull surface using a 26-gauge needle. Immediately thereafter the incision was closed with surgical adhesive and the animals were monitored until conscious and returned to their cages. Animals were randomly assigned to control, TMZ treated group (120 mg/kg/d), CAT_3 low-dose group (6 mg/kg/d) and CAT_3 high-dose group (12 mg/kg/d) (n=3). From the 15th day of the operation, mice in CAT_3 low-dose groups and CAT_3 high-dose groups were treated of CAT_3 orally; and mice in TMZ group were treated of TMZ orally.

Imaging analysis. All mice experienced high resolution MR (Bruker, Bremen, Germany) scanning weekly after operation. The MR images (Siemens, Munich, Germany) were acquired using a 1.5 tesla clinical unit. The slice thickness for coronal and transverse scan was 0.5 mm. The mice were anesthetized with intraperitoneal injection of pentobarbital sodium solution in a dosage of 50 mg/kg. After coronal and transverse T2 weighted images had been obtained, coronal plane enhanced T1 weighted images were acquired by an intravenous injection of dimeglumine gadopentetate (Magnevist, Bayer Schering Parma, Germany) at a dose of 2 ml/kg body weight via caudal vein.

Table I. Anti-proliferative activity of PF403 on SHSY-5Y cells by MTT assay.

Time (h)	IC_{50} (M)	
	PF403	Taxol
48	$5.25\pm1.41\times10^{-6}$	$1.57\pm0.42\times10^{-4}$
72	$4.21\pm1.23\times10^{-11}$	$5.16\pm2.24\times10^{-8}$
96	$2.84\pm1.13\times10^{-12}$	$2.61\pm1.43\times10^{-8}$

SH-SY5Y cells were treated with 5×10^{-5}-1×10^{-13} M of PF403. Taxol was used as a positive control, and DMSO treated cells were considered as controls. After 48, 72 and 96 h of treatment, IC_{50} values were calculated.

Histopathological analysis. Paraffin-embedded mouse whole brain. The thickness of sections was 5 μm. Serial sections were also stained with H&E. The stained images of each section were acquired using a microscope (Nikon, Tokyo, Japan). H&E staining was used in diagnosis, and analysis of the pathology changes.

Western blot analysis. For western blotting, samples transferred to a nitrocellulose membrane by semi-wet electrophoresis were subjected to SDS-PAGE and incubated with primary antibody rabbit anti-FAK, rabbit anti-phosphorylated FAK, rabbit anti-MMP-2, rabbit anti-MMP-9, rabbit anti-PI3K p85, rabbit anti-phosphorylated PI3K p85, rabbit anti-AKT, rabbit anti-phosphorylated AKT, rabbit anti-mTOR, rabbit anti-phosphorylated mTOR, rabbit anti-c-Raf, rabbit anti-phosphorylated c-Raf, rabbit anti-MEK, rabbit anti-phosphorylated MEK, rabbit anti-ERK, rabbit anti-phosphorylated ERK1/2, rabbit anti-Mcl1, rabbit anti-Bcl-2, rabbit anti-BAX, mouse anti-Bad, mouse anti-Bid, mouse anti-Bim, rabbit anti-caspase-9, rabbit anti-cleave caspase-9, rabbit anti-caspase-3, rabbit anti-cleave caspase-3, rabbit anti-PARP and rabbit anti-cleave PARP antibodies (Cell Signaling Technology, Danvers, MA, USA) overnight at 4˚C. The samples were detected with horseradish peroxidase-conjugated anti-rabbit or anti-mouse IgG (Cell Signaling Technology) and developed using an ECL. Membranes were tested for equal loading by probing for actin.

Statistical analysis. The results were expressed as means ± SD for repeated measures, and t-test was used for comparison of differences between groups. Differences were considered statistically significant when $P\leq0.05$.

Results

PF403 induces cytotoxicity in SH-SY5Y neuroblastoma cells in a dose- and time-dependent manner. The MTT assay, colony forming assay and flow cytometry assay were chosen to test the cytotoxicity of PF403 in NB. Administration with different concentrations of PF403 (5×10^{-5}-5×10^{-13} M) for 48 h, 72 and 96 h, cell viability was determined using MTT assay. The viability of the untreated cells was regarded as 100%. The results revealed that PF403 could inhibit SH-SY5Y cell proliferation significantly from 48 to 96 h, and its potency

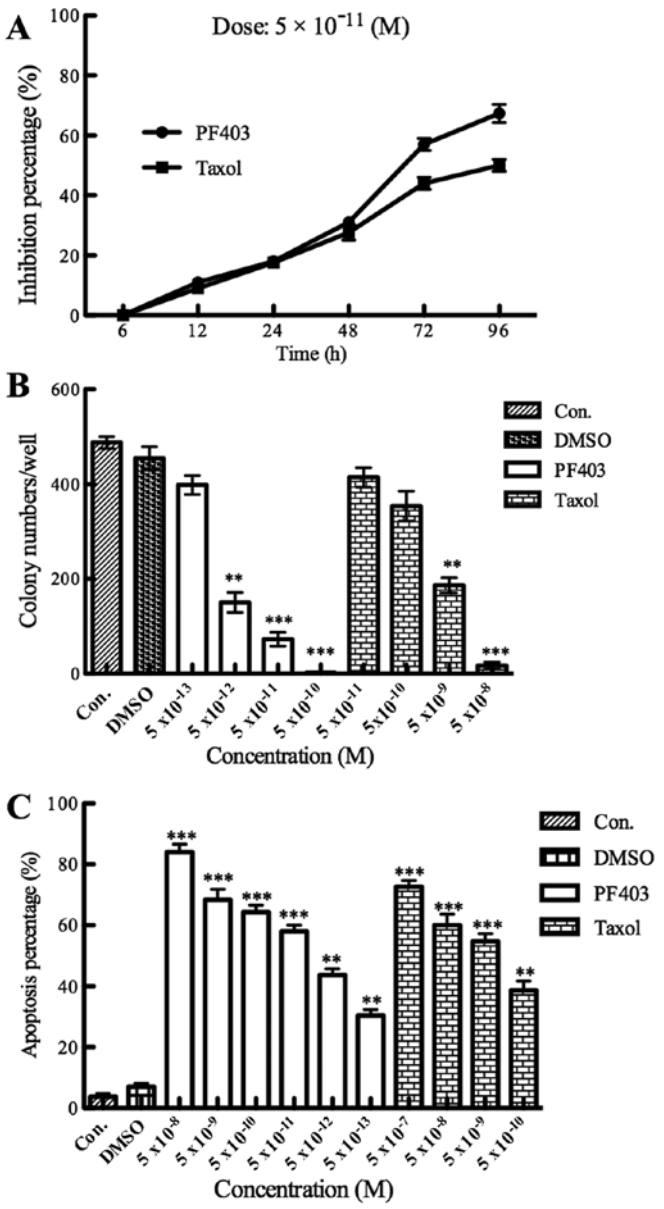

Figure 2. (A) The time-dependent curve of PF403 at the concentration of 5×10^{-11} M. SH-SY5Y cells were treated with 5×10^{-11} M of PF403 and Taxol. DMSO treated cells were considered as controls. After 6, 12, 24, 48, 72 and 96 h of treatment, the inhibition percentages were detected by MTT assay. (B) Anti-proliferative effect of PF403 on SH-SY5Y NB cells by colony formation assay. The concentrations of PF403 was 5×10^{-10}-5×10^{-13} M. As the results show, PF403 suppressed colony formation ability of SH-SY5Y NB cells. The IC_{50} value was $3.81\pm1.29\times10^{-13}$ M. (C) Apoptosis of SH-SY5Y cells treated with PF403 for 72 h by flow cytometry. SH-SY5Y cells were treated with PF403 (5×10^{-8}-5×10^{-13} M) for 72 h. Taxol (5×10^{-7}-5×10^{-10} M) was used as a positive control. The ordinate shows the population of apoptotic cell groups. The IC_{50} was 10^{-11} M. The data are presented as the mean ± standard deviation. $^{*}P<0.05$, $^{**}P<0.005$, $^{***}P<0.001$, compared with the control group.

was higher than taxol (Table I). The time-dependent curve of MTT assay demonstrated the concentration of PF403 at 5×10^{-11} M, its proliferation inhibitory ability in SH-SY5Y cells reached stable stage after 72 h, and PF403 had stronger antitumor proliferation ability than taxol after 48 h (Fig. 2A). The results of PF403 on proliferation were confirmed by the colony formation assay, the IC_{50} of PF403 was $3.81\pm1.29\times10^{-13}$ M, and the IC_{50} of taxol was $4.77\pm1.29\times10^{-9}$ M (Fig. 2B).

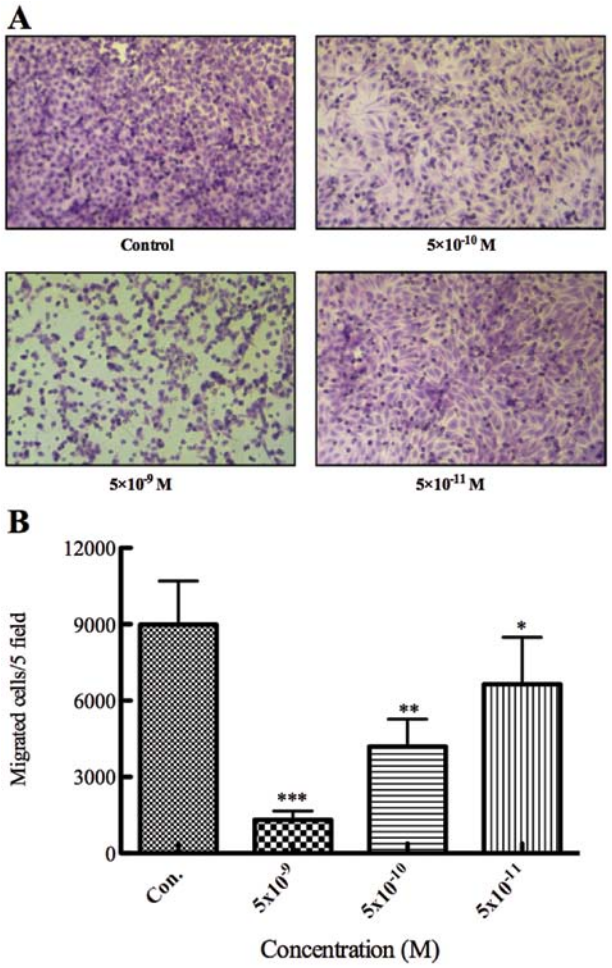

Figure 3. PF403 affects the invasion capacity of SH-SY5Y cells. SH-SY5Y cells were treated with concentrations ($5x10^{-9}$ M, $5x10^{-10}$ M and $5x10^{-11}$ M) of PF403 for 24 h. The data are presented as the mean ± standard deviation. *P<0.05; **P<0.005; ***P<0.001, compared with the control group (magnification, x100).

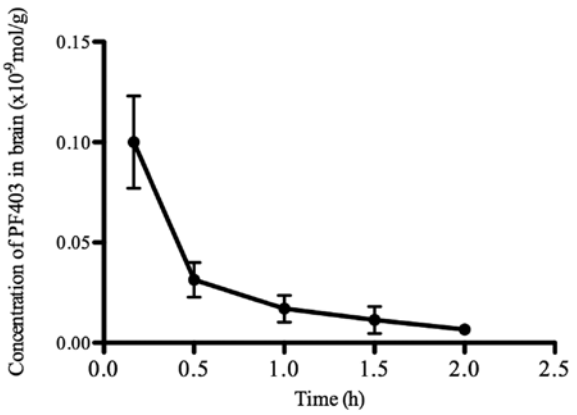

Figure 4. Concentration of PF403 in brain after CAT_3 oral administration for 5 min. Line equation of concentration of PF403 in brain tissue was: Y = 0.000474 xX+0.000611, R2=0.9985 (1-500 ng/ml). PF403 was detected in brain tissue after CAT_3 oral administration for 5 min, and peak time was 5 min-1 h, the average concentration of peak was 3.87~34.17 pg/ml.

Table II. PF403 affected the invasion capacity in SH-SY5Y cells.

Groups	Concentration (M)	Cell count	Inhibition rate (%)
Control	-	8981±1710	-
PF403	$5x10^{-9}$	1313±355[a]	83.36
	$5x10^{-10}$	4192±1087[a]	53.34
	$5x10^{-11}$	6648±1836[b]	26.06

SH-SY5Y cells were treated with concentrations of PF403 for 24 h. Results were reported as mean migrated cells/5 field ± SD of three independent experiments. The inhibition rate was calculated according to the formula: Inhibition rate = (Cell count (Control)-Cell count (PF403))/Cell count (Control). [a]P<0.001; [b]P<0.005.

The results of flow cytometry displayed that the apoptotic cells were increased dramatically in PF403 treated groups compared with control and DMSO groups, the IC_{50} was at 10^{-11} M (Fig. 2C). These results preliminarily demonstrated that PF403 had a strong anti-NB activity *in vitro*.

PF403 inhibits invasion of SH-SY5Y cells. To investigate the effect of PF403 on invasion in SH-SY5Y cells, we treated the SH-SY5Y NB cancer cells with various concentrations of PF403 for 24 h and observed cell invasion by Transwell assay. The results indicated that the dose required for inhibition of SH-SY5Y cell invasion was much less than the dose needed to cause apoptosis (IC_{50} value at 10^{-3} M, at 24 h) (Table II and Fig. 3). These results suggested that PF403 was able to affect invasion ability of SH-SY5Y neuroblastoma cells at a low concentration.

CAT_3 metabolizes into PF403 in vivo. There was no significant change in the concentration of CAT_3 and PF403 incubated with artificial gastric juice for 15 min. However, the concentrations of CAT_3 were reduced, and PF403 could be detected while incubated with hepatic microsome, plasma or artificial intestinal fluid for 15 or 20 min. CAT_3 (59%) metabolized into PF403 after incubated with artificial intestinal fluid for 15 min. PF403 was detected in brain tissue after CAT_3 oral administration for 5 min (Fig. 4). These results demonstrated that CAT_3 metabolized into PF403 *in vivo*, and PF403 was proved to penetrate the blood-brain barrier.

The pro-drug of PF403 and CAT_3, has a potent anti-neuroblastoma activity in situ. In order to observe the anti-neuroblastoma activity of PF403 *in vivo*, an *in situ* model was enrolled. The pro-drug of PF403, CAT_3, was utilized to improve the bioavailability. MRI was chosen to observe the development of tumor in brain, and H&E staining in diagnosis and in analysis of the tumor. Coronal plane T2 weighted images demonstrated mildly hyper-intense intracranial tumor and hard to observe invasion of the surrounding brain tissue of mice in the experimental group. Control group T2 weighted images showed larger area of hyper-intense intracranial tumor than the experimental groups, and clear invasion of the surrounding brain tissue (Fig. 5A). Coronal plane enhanced T1 weighted images demonstrated markedly small intracranial tumors of mice

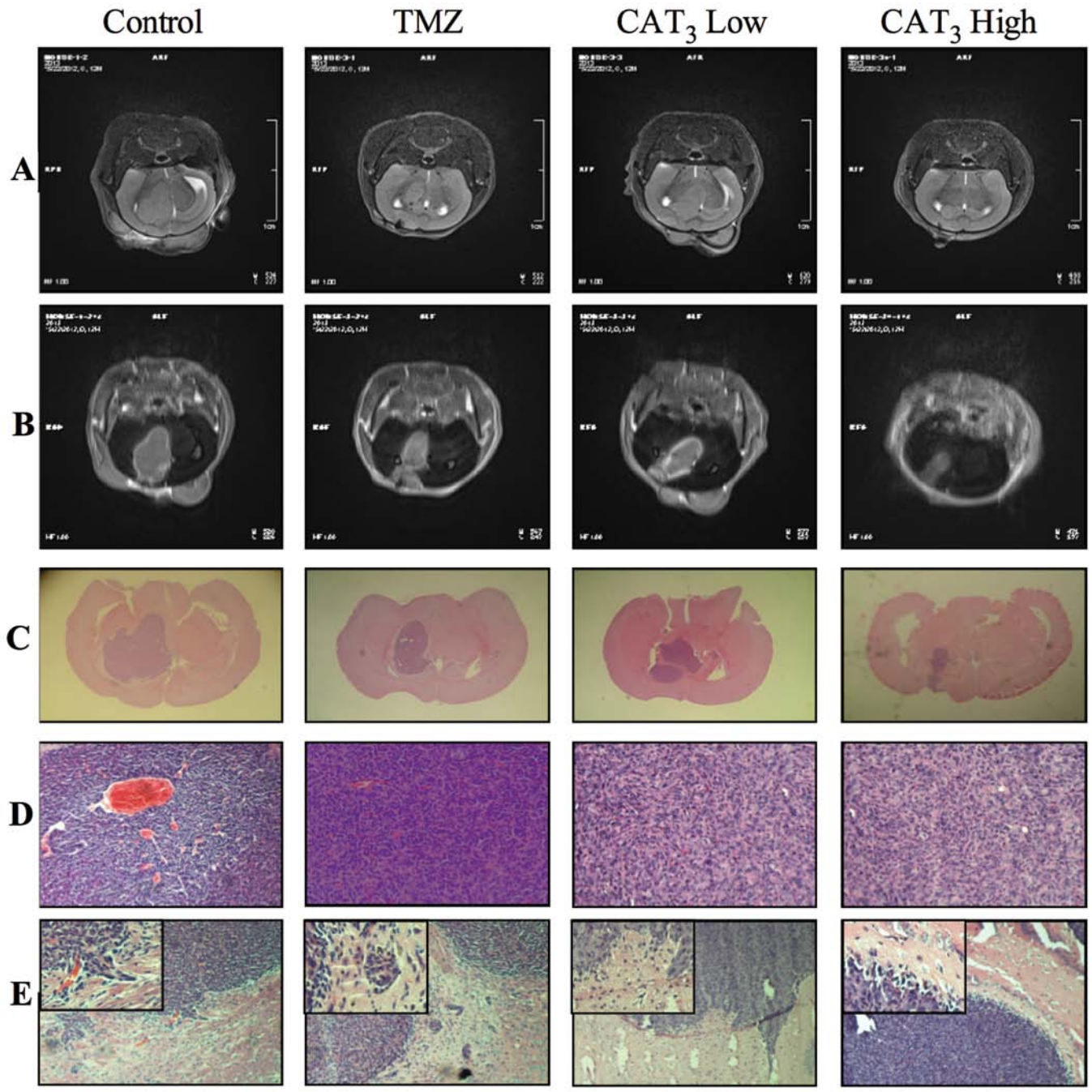

Figure 5. (A) Coronal plane T2 weighted images. (B) Contrast enhancement of T1 weighted images. (C) H&E stains of brain tissue. (D) H&E stains of neuroblastoma cells (magnification, x100). (E) CAT_3 inhibited invasion ability of SH-SY5Y neuroblastoma cells. H&E stain showed the morphology and invasion of SH-SY5Y neuroblastoma cells. Neovascularization was common in control and TMZ treated groups. In histology, undifferentiated and low differentiated types were common in the control group, but well-differentiated type was dominant in CAT_3 treated groups. Neuroblastoma cells in control and TMZ treated groups invaded into the tissue, but tumors in CAT_3 treated groups had a clear fibrotic boundary.

in the experimental group, whereas tumors occupied almost the whole brain of mice in the control group (Fig. 5B). Tumor was observed in 9 successive slices for control group, and 8 slices for TMZ (120 mg/kg) group, but only 6 and 4 slices for CAT_3 low group (6 mg/kg) and CAT_3 high group (12 mg/kg). Histopathological examination of control mice showed that experimental groups developed smaller tumors in the brain (Fig. 5C). H&E staining proved the tumor as neuroblastoma, tumor cells packed closely, cell morphology was basically the same, mostly the small round cells were distributed like islands. Shape and boundary of the tumors were consistent with MRI results. The tumor cells had less cytoplasm and their nucleus was clear. Capillaries surrounding tumor cells were arranged in a rosette structure (Fig. 5D). Tumor cells invaded into the surrounding normal tissue, but in CAT_3 treated groups this phenomenon was not observed (Fig 5E). The volume of tumor through MRI and H&E stain sections were calculated, and showed consistency of the two methods (Table III). These results proved that the pro-drug of PF403 had potent anti-neuroblastoma activity *in situ*.

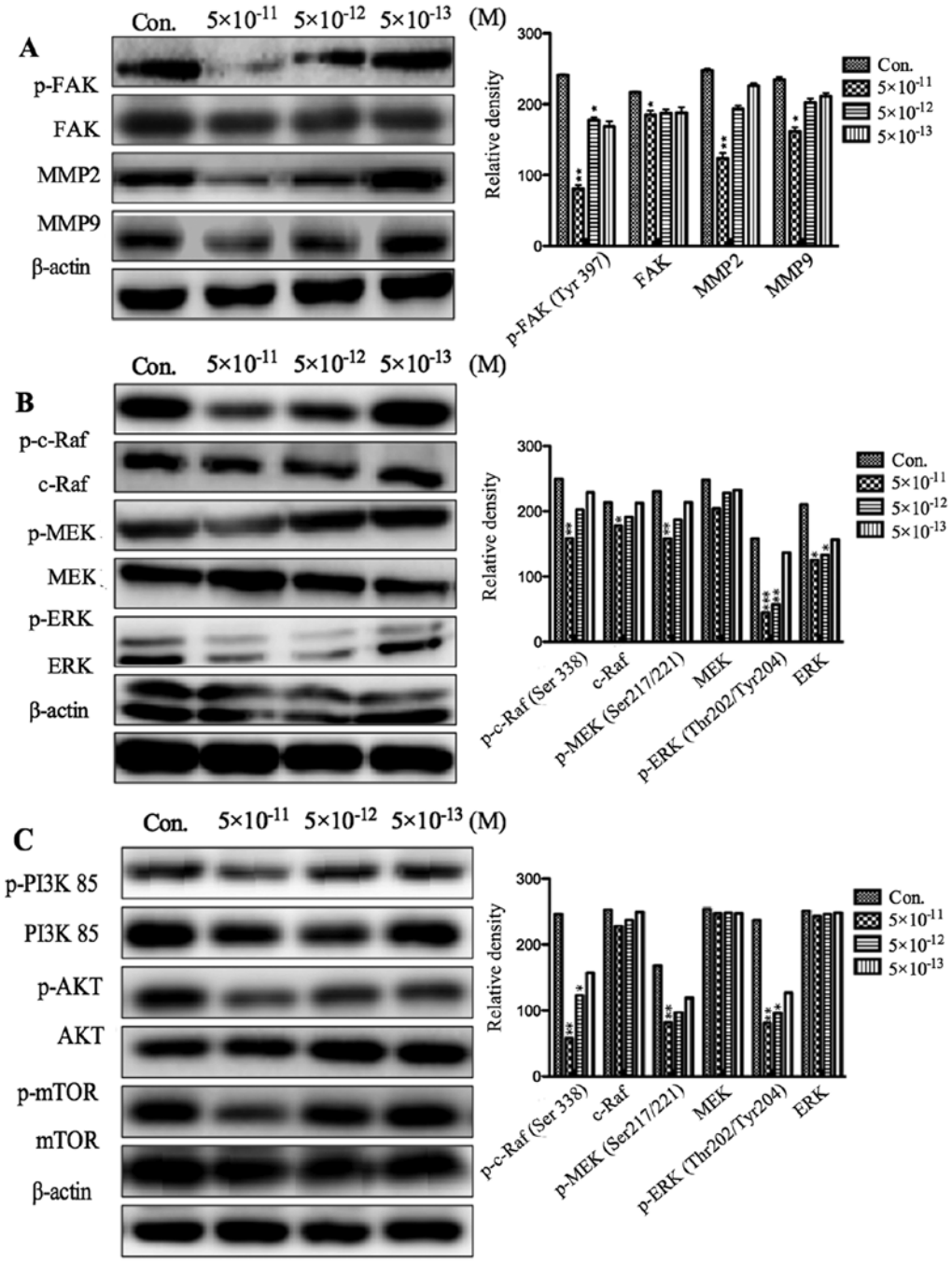

Figure 6. (A) PF403 affected invasion proteins expression on SH-SY5Y cells at 4 h. (B) PF403 affected Raf/MEK/ERK signaling on SH-SY5Y cells at 4 h. (C) PF403 affected PI3K/AKT/mTOR signaling on SH-SY5Y cells at 4 h. SH-SY5Y cells were cultured and treated with $5x10^{-9}$ M, $5x10^{-10}$ M and $5x10^{-11}$ M of PF403 for 4 h, and cell lysates immunoblotted with antibodies. Blots were stripped and immunoblotted with anti-β-actin antibody. The results clearly indicated p-FAK, MMP-2, MMP-9, proteins of Raf/ERK and PI3K/AKT pathways was downregulated in PF403 treated cells for 4 h. $^{*}P<0.05$, $^{**}P<0.005$ and $^{***}P<0.001$.

PF403 induces the change of multiple cell signaling pathways involved in tumor cell invasion and cell apoptosis. We explored which factors were involved in the events where PF403 inhibited invasion and induced apoptosis of neuroblastoma cells. In the process of tumor cell invasion, focal adhesion kinase (FAK) and matrix metalloproteinases (MMPs) play an important role (10). The levels of MMP-2, MMP-9, phosphorylated and total FAK in PF403 ($5x10^{-11}$ M, $5x10^{-12}$ M and $5x10^{-13}$ M) treated SH-SY5Y cells were detected by western blot analysis at different times. The results showed that the expression of p-FAK, MMP-2 and MMP-9 was, respectively, significantly decreased after treatment with PF403 for 4 and 72 h (Figs. 6A and 7A). However, the total of FAK did not alter (Figs. 6A and 7A). The expression of FAK is related to the Ras-mitogen-activated protein kinases (MAPKs) and PI3K/AKT cell signaling pathway (11,12). To assess whether the PF403 inhibited phosphorylation of FAK was associated with these cell signaling pathways, SH-SY5Y cells were treated with various concentrations of PF403 ($5x10^{-11}$ M, $5x10^{-12}$ M and $5x10^{-13}$ M) for 4 and 72 h. The results of protein expression of Raf/MEK/ERK and PI3K/AKT/mTOR pathway demonstrated that PF403 downregulated the proteins expression

Table III. Antitumor activity of CAT_3 on neuroblastoma *in situ*.

Groups	Body weight		H&E staining				MRI				
	Beginning	End	Lmax (mm)	W (mm)	V_H (mm)	Inhibition rate (%)	Lmax (mm)	W (mm)	T (mm)	V_M (mm)	Inhibition rate (%)
Control	16.2±0.9	17.3±2.9	5.4±1.3	4.4±1.6	104.5	-	5.2±2.1	3.7±1.1	4.5±0.5	86.6	-
TMZ	16.7±1.1	17.5±2.1	4.3±1.2	2.4±1.0	24.8[a]	76.3	3.9±1.3	2.4±0.8	4.0±0.5	37.4[a]	56.8
CAT_3 low	16.5±1.1	17.7±2.3	4.0±1.5	3.1±1.1	38.4[a]	63.3	3.9±1.1	2.9±0.9	3.0±0.5	33.9[a]	60.9
CAT_3 high	16.3±1.2	17.9±1.9	2.8±1.0	1.7±0.6	8.1[a]	92.2	2.7±1.1	2.0±0.5	2.0±0.5	10.8[a]	87.5

There was no significant body weight loss, or death, after oral administration of CAT_3 and TMZ for 8 days successive. Lmax is the maximum length in the maximum cross-sectional tumor with H&E staining. W is the maximum wide perpendicular to the Lmax. In the MR imaging, Lmax and W were measured as the H&E staining, and T (thickness) was calculated by number of splices multiplying the thickness of the splice. H&E stained tumor volume formula was $V_H = L_{max} \times W^2$, and MRI tumor volume calculation was $V_M = L_{max} \times W \times T$. [a]P<0.001.

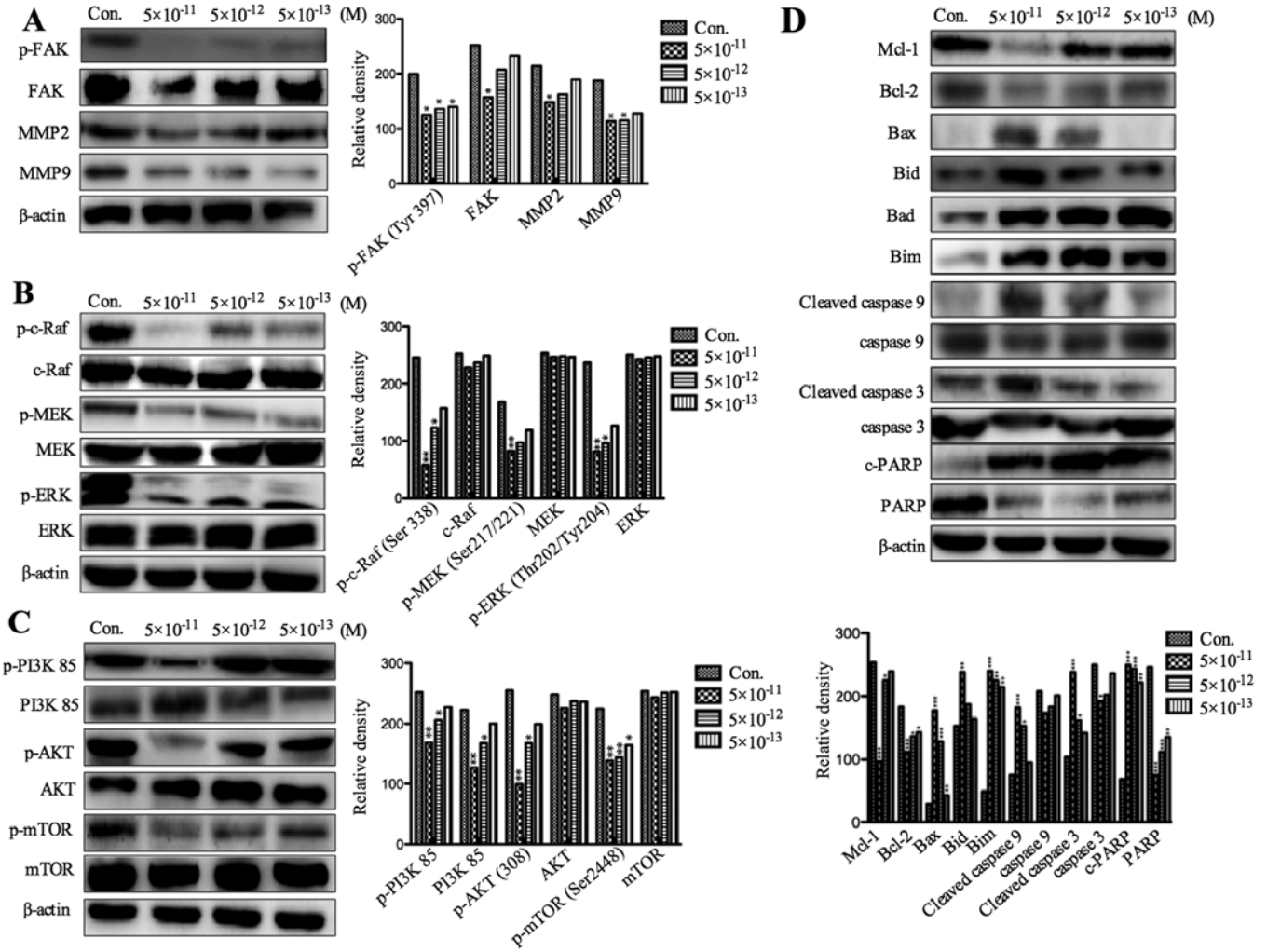

Figure 7. (A) PF403 affected invasion protein expression on SH-SY5Y cells at 72 h. (B) PF403 affected Raf/MEK/ERK signaling on SH-SY5Y cells at 72 h. (C) PF403 affected PI3K/AKT/mTOR signaling on SH-SY5Y cells at 72 h. (D) PF403 affected apoptosis protein expression on SH-SY5Y cells at 72 h. SH-SY5Y cells were cultured and treated with $5x10^{-11}$ M, $5x10^{-12}$ M and $5x10^{-13}$ M of PF403 for 72 h, and the cell lysates immunoblotted with antibodies. Blots were stripped and immunoblotted with anti-β-actin antibody. The results clearly indicate p-FAK, MMP-2, MMP-9, proteins of Raf/ERK, PI3K/AKT, apoptosis pathway was downregulated in PF403 treated cells in 72 h. **P<0.05, **P<0.005 and **P<0.001.

of Raf/MEK/ERK and PI3K/AKT/mTOR pathways at the concentration of $5x10^{-11}$ M in 4 h (Fig. 6B and C), and PF403 downregulated proteins expression of Raf/MEK/ERK and PI3K/AKT/mTOR pathway at $5x10^{-13}$ M for 72 h in a concen-

tration dependent manner (Fig. 7B and C). PF403 accelerated apoptosis by upregulated expression of pro-apoptotic proteins (Bad, Bid, Bim and Bax), downregulated anti-apoptosis proteins (Mcl-1 and Bcl-2), and activated caspase-dependent mitochondrial apoptosis pathways (cleave-caspase-9, cleave-caspase-3 and c-PARP) in cells administrated with PF403 for 72 h (Fig. 7D).

Discussion

The clinical characteristics of NB are heterogeneity, metastasis and high malignancy, resulting in shorter survival in patients (2,13). Few chemotherapeutic or molecularly targeted antineoplastic agents have shown efficacy in brain tumors, therefore, development of novel chemotherapy agents are urgent. Our earlier study had found that PF403 exerted potent antitumor activity in various tumors *in vitro*, such as, melanoma, hepatoma, ovarian cancer, glioma and neuroblastoma (9). As this compound could penetrate the blood-brain barrier (8), we supposed that it could suppress growth of brain tumors, and neuroblastoma was chosen in this study. The results of MTT, colony formation and flow cytometry illustrated that PF403-induced SH-SY5Y cell death was dose- and time-dependent. Significant increase in cell deaths was observed at the lowest concentration of PF403 treated groups than controls. PF403 induced SH-SY5Y cell apoptosis with EC_{50} value of 10^{-11}-10^{-12} M at 72 h by MTT assay. This is much lower than its precursor compound CAT (at 72 h IC_{50} value was 10^{-7}-10^{-8} M) (7), and the traditional cytotoxic drug taxol (at 72 h IC_{50} value at 10^{-8}-10^{-9} M). Colony forming assay showed that PF403 inhibited SH-SY5Y NB cell proliferation in a long-term, and it had a good dose-effect relationship. Flow cytometry assay showed that SH-SY5Y cells cultured with PF403 for 72 h induced intense apoptosis.

Invasion of growth is the most characteristic biological phenotype of NB, which is also the major reason causing poor prognosis. The present study found that PF403 could inhibit the invasion ability of NB cells in a dose-dependent manner, which is essential for NB treatment.

As PF403 displayed a strong anti-neuroblastoma and anti-invasion activity *in vitro*, subsequently its antitumor activity *in vivo* was studied. The barrier function of the BBB is critical for regulating transport to the brain, but also represents a significant roadblock in developing therapies for CNS diseases including brain cancer, and most convention of chemotherapeutic agents cannot penetrate BBB (14-16). Besides, the microenvironment in brain is different from other tissues in human body. Thus, an *in situ* NB model was used to evaluate the proliferation inhibitory activity of PF403. Our results exhibited that, 14 days after SH-SY5Y cell implantation, the tumor could be located by MRI in mouse brain, and CAT_3 significantly inhibited NB cell proliferation. H&E staining confirmed its potent anti-proliferation and anti-invasion ability *in situ*.

FAK is a mediator of cell-extracellular matrix signaling events and its expression plays an important role in the process of NB invasion (17). Compiling evidence implies that FAK regulates focal adhesion signaling by phosphorylating various substrates, as well as the MMPs-mediated matrix degradation, which consecutively regulates downstream signaling cascades (18). FAK signaling played a critical role in the production of MMPs such as MMP-2 and MMP-9, and subsequently activated tumor invasion (10). Sun *et al* (19) demonstrated that inhibition of the expression and phosphorylation of FAK, activities of MMP-2 and MMP-9 could be downregulated. FAK is also essential for the Ras/ERK signaling pathway (20). The residues surrounding Tyr^{397} (FAK) can also constitute a sequence that binds to the Ras/ERK signaling pathway (21). FAK and MAPK signaling involved in MMP-2 secretion has been shown in QG90 lung cancer cell (22). Moreover, it was found that the MMP-9 gene promoter is partially regulated through activation of the Ras/ERK pathway (23). Also, PI3K is one of the critical downstream signal molecules of the FAK pathway (24). Activated FAK binds the SH2 of PI3K, thereby transporting the catalytic subunit of PI3K to the membrane, where it catalyzes the phosphorylation of inositol lipids in lung cancer cell migration (25). Several studies have indicated that FAK/PI3K/Akt is involved in the regulation of MMP-2 and MMP-9 activities on different cell types (12,26). In the present study, PF403 inhibited the activation of FAK, reduced phosphorylation of FAK, and regulated the expression of MMP-2 and MMP-9. In addition, it showed that PF403 inhibited PI3K/AKT/mTOR and Raf/MEK/ERK pathways in SH-SY5Y cells. Thus, it seems that PF403 inhibited SH-SY5Y NB cell migration in concert with downregulated protein expression of PI3K/AKT and Raf/ERK signaling pathways, and associated with p-FAK, MMP-2 and MMP-9.

PI3K/AKT/mTOR and Raf/MEK/ERK pathways influence protein expression of the Bcl-2 family, they play a central role in apoptosis by regulating mitochondrial outer membrane permeabilisation (MOMP) and releasing apoptosis-inducing proteins such as cytochrome *c*, and SMAC sequestered within the mitochondria (27). The Bcl-2 family is divided into three groups based on functionality and presence of conserved Bcl-2 homology (BH1-4) domains: multi-domain anti-apoptotic proteins (Bcl-2 and Mcl-1), multi-domain pro-apoptotic proteins (BAX) and BH3-only proteins (Bad, Bid and Bim). Interactions between these groups of proteins dictate whether the cells die or not. Multi-domain anti-apoptotic proteins prevent MOMP by interacting with and sequestering the multi-domain pro-apoptotic proteins (28,29). BAX allows for oligomerization at the mitochondrial outer membrane and subsequent MOMP through pore formation (30). The BH3-only proteins, competitively bind and neutralize anti-apoptotic proteins, allowing BAX oligomerization and promoting cell death, whereas Bid and Bim can also interact with and activate BAX, facilitating membrane insertion and MOMP (27,31). In this study, upregulation of BAX and downregulation of Bcl-2 was observed in a PF403 concentration-dependent manner. PF403 could upregulate expression of Bim, Bid and Bad, and downregulate expression of Mcl1. The regulation of expression of the Bcl-2 family proteins was a response to the accelerated SH-SY5Y cell death.

Apoptotic pathways in PF403-mediated cell death in SH-SY5Y neuroblastoma cells were examined. The activity of PI3K/AKT and Ras/ERK pathways was downregulated in PF403 treated cells, which were important to proliferation and apoptosis of NB. Our results also strongly demonstrated caspase-9, downstream of Bcl-2 family, was activated in PF403 treated SH-SY5Y cells, suggesting activation of the intrinsic

apoptotic pathway. Downstream target of caspase-9, caspase-3, was also activated in PF403 treated SH-SY5Y cells. Activation of caspase-3 has been reported to have targets in nuclear compartment for the initiation of DNA damage suggesting its nuclear localization (32). PARP is a nuclear target of cleaved caspase-3 and proteolysis cleavage of PARP is considered to be a hallmark feature of apoptosis. Our results demonstrated the presence of only full-length PARP protein in untreated cells but a strong PARP fragment was produced in all PF403 treated cells, strongly suggesting involvement of apoptosis. Taken together, our results clearly suggest that the intrinsic apoptotic pathway was contributed to PF403-mediated SH-SY5Y cell death.

In conclusion, the results presented in the present study demonstrated the effect and novel mechanisms associated with cytotoxic property of PF403 on NB cells. Our studies show that PF403, a novel antitumor agent, could induce apoptosis and inhibit invasion and metastasis of SH-SY5Y NB cells *in vitro*; CAT_3, the pro-drug of PF403, had anti-neuroblastoma activity *in situ*; PF403 inhibited invasion of NB cells through downregulating protein expression of p-FAK, following MMP-2, MMP-9 and Raf/ERK and PI3K/AKT pathways; PF403-mediated neuroblastoma cell death partly through downregulating Raf/MEK/ERK and PI3K/AKT/mTOR pathways, and then activating apoptotic pathway through regulation of proteins expression of Bcl-2 family activating the intrinsic apoptotic pathway. Thus, the primary biochemical mechanism of action of PF403 was as speculated. In summary, our results strongly suggested that PF403 has potential as a new anticancer drug for the treatment of neuroblastoma.

References

1. Brodeur GM: Neuroblastoma: biological insights into a clinical enigma. Nat Rev Cancer 3: 203-216, 2003.
2. Maris JM, Hogarty MD, Bagatell R and Cohn SL: Neuroblastoma. Lancet 369: 2106-2120, 2007.
3. Chemler SR: Phenanthroindolizidines and phenanthroquinolizidines: promising alkaloids for anti-cancer therapy. Curr Bioact Compd 5: 2-19, 2007.
4. Fu Y, Lee SK, Min HY, Lee T, Lee J, Cheng M and Kim S: Synthesis and structure-activity studies of antofine analogues as potential anticancer agents. Bioorg Med Chem Lett 17: 97-100, 2007.
5. Gao W, Bussom S, Grill SP, Gullen EA, Hu YC, Huang X, Zhong S, Kaczmarek C, Gutierrez J, Francis S, *et al*: Structure-activity studies of phenanthroindolizidine alkaloids as potential antitumor agents. Bioorg Med Chem Lett 17: 4338-4342, 2007.
6. Xi Z, Zhang R, Yu Z and Ouyang D: The interaction between tylophorine B and TMV RNA. Bioorg Med Chem Lett 16: 4300-4304, 2006.
7. Liu ZJ, Lv HN, Li HY, Zhang Y, Zhang HJ, Su FQ, Si YK, Yu SS and Chen XG: Anticancer effect and neurotoxicity of S-(+)-deoxytylophorinidine, a new phenanthroindolizidine alkaloid that interacts with nucleic acids. J Asian Nat Prod Res 13: 400-408, 2011.
8. Lv H, Ren J, Ma S, Xu S, Qu J, Liu Z, Zhou Q, Chen X and Yu S: Synthesis, biological evaluation and mechanism studies of deoxytylophorinine and its derivatives as potential anticancer agents. PLoS One 7: e30342, 2012.
9. Yu P, Li C, Ren J, Ma S, Song X, Chen X and Yu S: Stereospecific synthesis and biological evaluation of monodesmethyl metabolites of (+)-13a-(S)-deoxytylophorinine as potential antitumor agents. Synthesis 44: 3757-3764, 2012.
10. Mon NN, Ito S, Senga T and Hamaguchi M: FAK signaling in neoplastic disorders: a linkage between inflammation and cancer. Ann NY Acad Sci 1086: 199-212, 2006.
11. Shibata K, Kikkawa F, Nawa A, Thant AA, Naruse K, Mizutani S and Hamaguchi M: Both focal adhesion kinase and c-Ras are required for the enhanced matrix metalloproteinase 9 secretion by fibronectin in ovarian cancer cells. Cancer Res 58: 900-903, 1998.
12. Zeng ZZ, Jia Y, Hahn NJ, Markwart SM, Rockwood KF and Livant DL: Role of focal adhesion kinase and phosphatidylinositol 3'-kinase in integrin fibronectin receptor- mediated, matrix metalloproteinase-1-dependent invasion by metastatic prostate cancer cells. Cancer Res 66: 8091-8099, 2006.
13. De Bernardi B, Nicolas B, Boni L, Indolfi P, Carli M, Cordero Di Montezemolo L, Donfrancesco A, Pession A, Provenzi M, Di Cataldo A, *et al*: Disseminated neuroblastoma in children older than one year at diagnosis: comparable results with three consecutive high-dose protocols adopted by the Italian Co-Operative Group for Neuroblastoma. J Clin Oncol 21: 1592-1601, 2003.
14. Pardridge WM: The blood-brain barrier: bottleneck in brain drug development. NeuroRx 2: 3-14, 2005.
15. Pardridge WM: Molecular Trojan horses for blood-brain barrier drug delivery. Curr Opin Pharmacol 6: 494-500, 2006.
16. Pardridge WM: Biopharmaceutical drug targeting to the brain. J Drug Target 18: 157-167, 2010.
17. Yount G, Taft RJ, Luu T, Rachlin K, Moore D and Zhang W: Independent motile microplast formation correlates with glioma cell invasiveness. J Neurooncol 81: 113-121, 2007.
18. Canel M, Secades P, Garzón-Arango M, Allonca E, Suarez C, Serrels A, Frame M, Brunton V and Chiara MD: Involvement of focal adhesion kinase in cellular invasion of head and neck squamous cell carcinomas via regulation of MMP-2 expression. Br J Cancer 98: 1274-1284, 2008.
19. Sun T, Zhao N, Ni CS, Zhao XL, Zhang WZ, Su X, Zhang DF, Gu Q and Sun BC: Doxycycline inhibits the adhesion and migration of melanoma cells by inhibiting the expression and phosphorylation of focal adhesion kinase (FAK). Cancer Lett 285: 141-150, 2009.
20. Mon NN, Hasegawa H, Thant AA, Huang P, Tanimura Y, Senga T and Hamaguchi M: A role for focal adhesion kinase signaling in tumor necrosis factor-alpha-dependent matrix metalloproteinase-9 production in a cholangiocarcinoma cell line, CCKS1. Cancer Res 66: 6778-6784, 2006.
21. Lai KC, Huang AC, Hsu SC, Kuo CL, Yang JS, Wu SH and Chung JG: Benzyl isothiocyanate (BITC) inhibits migration and invasion of human colon cancer HT29 cells by inhibiting matrix metalloproteinase-2/-9 and urokinase plasminogen (uPA) through PKC and MAPK signaling pathway. J Agric Food Chem 58: 2935-2942, 2010.
22. Zhang Y, Thant AA, Hiraiwa Y, Naito Y, Sein TT, Sohara Y, Matsuda S and Hamaguchi M: A role for focal adhesion kinase in hyluronan-dependent MMP-2 secretion in a human small-cell lung carcinoma cell line, QG90. Biochem Biophys Res Commun 290: 1123-1127, 2002.
23. Chang YM, Shih YT, Chen YS, Liu CL, Fang WK, Tsai CH, Tsai FJ, Kuo WW, Lai TY and Huang CY: Schwann cell migration induced by earthworm extract via activation of PAs and MMP-2/9 mediated through ERK1/2 and p38. Evid Based Complement Alternat Med 2011: 395458, 2011.
24. Choi YA, Lim HK, Kim JR, Lee CH, Kim YJ, Kang SS and Baek SH: Group IB secretory phospholipase A2 promotes matrix metalloproteinase-2-mediated cell migration via the phosphatidylinositol 3-kinase and Akt pathway. J Biol Chem 279: 36579-36585, 2004.
25. Meng XN, Jin Y, Yu Y, Bai J, Liu GY, Zhu J, Zhao YZ, Wang Z, Chen F, Lee KY, *et al*: Characterisation of fibronectin-mediated FAK signalling pathways in lung cancer cell migration and invasion. Br J Cancer 101: 327-334, 2009.
26. Chan KC, Ho HH, Huang CN, Lin MC, Chen HM and Wang CJ: Mulberry leaf extract inhibits vascular smooth muscle cell migration involving a block of small GTPase and Akt/NF-kappaB signals. J Agric Food Chem 57: 9147-9153, 2009.
27. Green DR and Kroemer G: The Pathophysiology of mitochondrial cell death. Science 305: 626-629, 2004.
28. Kuwana T and Newmeyer DD: Bcl-2-family proteins and the role of mitochondria in apoptosis. Curr Opin Cell Biol 15: 691-699, 2003.
29. Ren D, Tu HC, Kim H, Wang GX, Bean GR, Takeuchi O, Jeffers JR, Zambetti GP, Hsieh JJ and Cheng EH: BID, BIM, and PUMA are essential for activation of the BAX- and BAK-dependent cell death program. Science 330: 1390-1393, 2010.
30. Wei MC, Zong WX, Cheng EH, Lindsten T, Panoutsakopoulou V, Ross AJ, Roth KA, MacGregor GR, Thompson CB and Korsmeyer SJ: Proapoptotic BAX and BAK: a requisite gateway to mitochondrial dysfunction and death. Science 292: 727-730, 2001.
31. Yang E, Zha J, Jockel J, Boise LH, Thompson CB and Korsmeyer SJ: Bad, a heterodimeric partner for Bcl-XL and Bcl-2, displaces Bax and promotes cell death. Cell 80: 285-291, 1995.
32. Zhivotovsky B, Samali A, Gahm A and Orrenius S: Caspases their intracellular localization and translocation during apoptosis. Cell Death Differ 6: 644-651, 1999.